Optical Engineering

OpticalEngineering.SPIEDigitalLibrary.org

Numerical modeling of graphene-coated fiber optic surface plasmon resonance biosensor for BRCA1 and BRCA2 genetic breast cancer detection

Md. Biplob Hossain
Tarik Bin Abdul Akib
Lway Faisal Abdulrazak
Md. Masud Rana

SPIE.

Md. Biplob Hossain, Tarik Bin Abdul Akib, Lway Faisal Abdulrazak, Md. Masud Rana, "Numerical modeling of graphene-coated fiber optic surface plasmon resonance biosensor for BRCA1 and BRCA2 genetic breast cancer detection," *Opt. Eng.* **58**(3), 037104 (2019), doi: 10.1117/1.OE.58.3.037104.

Numerical modeling of graphene-coated fiber optic surface plasmon resonance biosensor for BRCA1 and BRCA2 genetic breast cancer detection

Md. Biplob Hossain,[a,*] Tarik Bin Abdul Akib,[b] Lway Faisal Abdulrazak,[c] and Md. Masud Rana[d]
[a]Jashore University of Science and Technology, Department of Electrical and Electronic Engineering, Jashore, Bangladesh
[b]Bangladesh Army University of Engineering and Technology, Department of Electrical and Electronic Engineering, Natore, Bangladesh
[c]Cihan University Slemani, Department of Computer Science, Sulaimaniya, Iraq
[d]Rajshahi University of Engineering and Technology, Department of Electrical and Electronic Engineering, Rajshahi, Bangladesh

Abstract. A numerical illustration of a hybrid design and numerical analysis of graphene-coated fiber-optic surface plasmon resonance (SPR) biosensor for BRCA-1 and BRCA-2 genetic breast cancer detection is provided. Two specific mutations named 916delTT in BRCA-1 gene and 6174delT in BRCA-2 gene are being selected for detection of breast cancer numerically. This sensor is based on attenuated total reflection (ATR) method to detect individual point mutations in BRCA-1 and BRCA-2 genes. Based on the numerically obtained results, a momentous change is present in the SPR angle (minimum 35% more) and surface resonance frequency (SRF) (minimum 36% more) for probe DNA with various concentrations of target DNA corresponding to the mutation of the BRCA-1 and BRCA-2 genes. The variation of the SPR angle and SRF for mismatched DNA strands in BRCA-1 and BRCA-2 genes is quite negligible, whereas that for complementary DNA strands is considerable. This considerable change is essential for proper detection of genetic biomarkers (916delTT and 6174delT) for early breast cancer. To the best of our knowledge, this is the first demonstration of such an adept biosensor for detecting BRCA1 and BRCA2 genetic breast cancer. Here, we used graphene as bimolecular acknowledgement element for improving sensor performance. At the end of the article, the performance in terms of sensitivity is analyzed. Therefore, the proposed biosensor opens a window toward detection of early detection of BRCA-1 and BRCA-2 genetic breast cancers. [DOI: 10.1117/1.OE.58.3.037104]

Keywords: attenuated total reflection; BRCA-1; BRCA-2; cancer; DNA hybridization; graphene; surface plasmon resonance; surface resonance frequency; 6174delT; 916delTT.

Paper 181830 received Dec. 28, 2018; accepted for publication Mar. 11, 2019; published online Mar. 27, 2019.

1 Introduction

The genetic tendency is responsible for 5% to 10% breast cancer and over 75% to 80% of inherited breast cancer cases are reported owing to mutations happening in BRCA1 and BRCA2 genes.[1,2] These genes are tumor suppressor associated with double strand DNA (dsDNA) repair accounts for abnormal uncontrolled tumor cell growth. Exceeding 400 different mutations in BRCA1 and BRCA2 genes leads to tumor growth and thus finally cancer.[3] Real-time detection of polymerase chain reaction (PCR) technologies has become the most traded and used for mutation detection with high specificity and sensibility.[3] Two prime factors, one is genetic and another is proteomic, are classified for breast cancer biomarkers. For example, BRCA1, BRCA2, and P53 are the genetic and ATM, CA125, CA153, CEA, CHEK2, HER-2, PTEN, and STK11 are the proteomic markers. These are responsible for breast cancer risk.[4,5] Every year above 350,000 deaths and 192,000 cases are reported due to breast cancer.[4] As yet, ultrasound, mammography, PCR screening, and other approaches have been applied to identify the diagnosis of breast cancer. This cancer cell is difficult to identify owing to tiny in size.[4,6] Thus, effective, precise approaches to breast cancer recognition and monitoring are immediately required.

A great deal of attention on surface plasmon resonance (SPR)-based biosensors as a leading optical sensing technology has been achieved by the researchers because of its applications in numerous fields, including medical diagnostics, biomolecule detection, biochemical detection, environmental monitoring, proteins–DNA hybridization, and DNA–DNA hybridization.[7–10] DNA hybridization is regularly used biomolecular method in which the level of genetic relationship between pools of DNA sequences to obtain the genetic gap between two organisms has been estimated.[11] This biochemical process of identifying DNA nucleotide bonding in proper orientation is very important for medical diagnostics.[6] This technology is being used to obtain information on DNA molecular bonding and, from here, BRCA1 and BRCA2 breast cancer directly diagnosable.

Fundamentally, SPR is a charge density oscillation between metal–dielectric interface stimulated by TM polarized electromagnetic waves, typically known as surface plasmon waves (SPW).[12,13] The SPW at the interface between a metal (e.g., Au, Ag, or Al) and a dielectric is used by the SPR biosensor to investigate the interactions between biomolecules.[8–13] And these interactions are accomplished by practice of optical fiber-based SPR sensors.[10] A fiber-optic

*Address all correspondence to Md. Biplob Hossain, E-mail: biplobh.eee10@gmail.com

0091-3286/2019/$25.00 © 2019 SPIE

SPR sensor for wavelength interrogation mode has lots of advantages, such as light in weight, compactness, high sensitivity, ease of multiplexing and remote sensing, mechanical flexibility, and the ability to transmit optical signals over a long distance, which allows miniaturization and chemical or biological sensing in inaccessible locations.[10] As a fundamental part of fiber optic SPR biosensor, a thin metallic film (Au, Ag, or Al) is coated with a fiber to distinguish the sensing medium and the dielectric.[12] Here, the sensing layer is used to functionalize the gold film, which consequently improves the absorption of biomolecules.[12–15]

An essential constituent of the SPR sensing device is large surface area-based absorbing material;[13] recently discovered 2-D nanomaterial graphene has satisfied this requirement regarding this Ref. 16. Graphene and graphene oxide facilitate biomolecule adsorption because of their large surface area and rich π conjugation structure,[17,18] making them suitable as dielectric top layers for SPR sensing.[19] Graphene has great fields of applications in advanced electronics, optoelectronics, and plasmonic due to exclusive characteristics of high carrier mobility, high optical transparency, exceptional mechanical flexibility, mechanical strength,[17–22] low resistivity, tunable conductivity, and extreme mode confinement.[23] Recent studies have focused graphene-based diverse applications in optoelectronic devices, including touch panels, ultrafast lasers, solar cells, optical modulators, photodetectors, and polarizers.[24,25] Graphene supports surface plasmons at terahertz frequencies that show larger confinement in comparison with other noble materials and lower losses due to longer electron relaxation times.[23] An important feature of graphene plasmons is tunable via gating or chemical doping.[26] This property can be applied in transformation optic devices, plasmonic switches, and planer lenses.[27]

In this paper, numerical modeling of a graphene-coated fiber optic SPR biosensor for breast cancer detection is reported. Since graphene has prominent characteristics, a graphene monolayer is sandwiched between gold film as an effective light absorption medium. We used $R_{\min} \sim \theta_{\mathrm{SPR}}$ (minimum reflectance versus SPR angle) as well as $T_{\max} \sim$ SRF (maximum transmittance versus SRF) as detecting attributors. This sensor is capable to recognize DNA hybridization event by checking the proper orientation of adenine (A), thymine (T), guanine (G), and cytosine (C) between immobilized mutant DNA sequence (sh-DNA) to mutated type complementary DNA (mr-DNA) in BRCA-1 and BRCA-2 gene shown in Figs. 2 and 3. The refractive index (RI) changes nearby the graphene and gold (Au) owing to the perfectly matched hybridization event between mr-DNA sequences of 916delTT and 6174delT biomarkers with sh-DNA sequence. The RI change will cause to turn a change in the propagation constant of the SPR wave, which can be optically ascertained by ATR method.[9,10] If significant change is present in $R_{\min} \sim \theta_{\mathrm{SPR}}$ as well as $T_{\max} \sim$ SRF curves, which indicates that perfectly matched complementary DNA hybridization has occurred between sh-DNA and mr-DNA sequences. And this significant change is the symptom for genetic breast cancer. If no significant change is found, it finally indicates no possibility of breast cancer. Phosphate-buffered saline (PBS) solution as bare sensing dielectric medium provides better adsorption of single-strand DNA biomolecules from mr-DNA sequences.[28,29] Our results demonstrated that SPR biosensors are able to detect mismatch sequences related to hereditary breast cancer with high sensitivity. We develop a pathological decision making table, whether there is breast cancer or not, on the basis of change minimum reflectance, SPR angle, maximum transmittance, and SRF. At the end of the article, we show the effect of adding graphene on the change of minimum reflectance, SPR angle, maximum transmittance, and SRF in terms of sensor sensitivity.

This paper is composed as follows: design methodology is given in Sec. 2. Section 2 consists of two subsections: one is mathematical modeling for proposed sensor and another is designated DNA sequences for detection of breast cancer. Section 3 discusses the details of the numerical results and discussions. Last, conclusion is given in Sec. 4.

2 Design Methodology

The proposed graphene implicated fiber optic SPR biosensor design structure is given in Fig. 1. Fiber optic SPR sensor has a core diameter of 50 μm[10] and cladding diameter of 50.25 μm. In sensor region, 5-mm cladding is detached and this slice of the cladding is considered to be implicated with a prism, gold (Au) thin film, and graphene with the thickness of dp = 74.5 nm,[10] $d_{\mathrm{Au}} = 50$ nm, and $d_g = 0.34$ nm $*$ £ (where £ is the total of graphene coatings), respectively.[9] This biosensor sensing region is involved with a total of four layers' Fresnel's structure.[9,12] The first layer is a SF11 prism having high RI; n_p of 1.723, the second layer is Au, deposited on the base of the prism having complex RI of $n_{Au} = 0.1726 + 3.4218i$. The third layer is a graphene having high complex RI; n_g of $3 + 1.149106i$ and the fourth layer is a

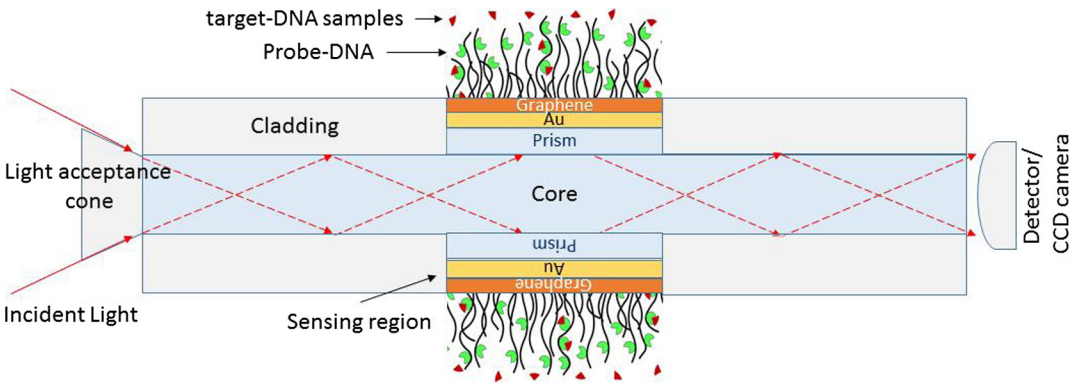

Fig. 1 Figural illustration of the four-layered model for fiber optic SPR biosensor: prism, Au (50 nm), graphene (0.34£ nm), and PBS contains p-DNA and complementary target mr-DNA or wt-DNA samples.

PBS solution as sensing dielectric medium for bare sensor cases.[9–14] The graphene-based biosensor as a adsorbing complementary molecule by the receptor produces a native increase in RI at the graphene to sensing medium inter-surface.[30] Once there is molecular interaction, the immobilization surface can be renewed by applying an appropriate chemical with the intention of eliminating target DNA samples except denaturing the probe DNA (p-DNA).[31]

In Fig. 1, light acceptance cone is the angle of an incident light hitting the fiber core and totally reflected by the cladding. In our proposed fiber optic SPR sensor, TM polarized He–Ne (wavelength, $\lambda = 633$ nm) light is used as an incident light.[9–12] The numerical results suggest that 633 nm allows the increased overall sensitivity of the sensor with the minimal possible Kerr effect.[32]

2.1 *Mathematical Modeling for Proposed Sensor*

The light is launched into one end and the power available of the other end (dP_T) at incident angle θ can be expressed as follows:[10,11]

$$dP_T \propto \left[\frac{n_c^2 \sin\theta \cos\theta}{(1 - n_c^2 \cos^2\theta)^2}\right] d\theta, \tag{1}$$

where n_c (1.451[10]) is the RI of the fiber core. The normalized transmitted power of p polarized TM light is expressed at the core–prism–metal try interface as follows: [10,11]

$$P_T = \frac{\int_{\theta_{cr}}^{\Pi/2} R_P^{\left(\frac{L}{D\tan\theta}\right)} \left[\frac{n_c^2 \sin\theta\cos\theta}{(1-n_c^2\cos^2\theta)^2}\right] \mathrm{d}(\theta)}{\int_{\theta_{cr}}^{\Pi/2} \left[\frac{n_c^2 \sin\theta\cos\theta}{(1-n_c^2\cos^2\theta)^2}\right] \mathrm{d}(\theta)}, \tag{2}$$

where L (5 mm) is the length of the sensing region, $D(50\ \mu\mathrm{m})$ is the diameter of the fiber core, and θ_{cr} is the critical angle of the optical fiber [expressed as $\theta_{cr} = a\sin(n_{cl}/n_c)$[10]], where n_{cl} is the RI of the fiber cladding. The reflected power R can be obtained by four-layered (prism, gold, graphene, and sensing layer) Fresnel's model analysis as follows:[9,12]

$$R = \frac{A + \frac{B}{Z_f} - Z_i\left(C + \frac{D}{Z_f}\right)}{A + \frac{B}{Z_f} + Z_i\left(C + \frac{D}{Z_f}\right)}, \tag{3}$$

where, Z_i and Z_f are initial (fiber core) and final layer (sensing layer) wave impedances, respectively, in the structure of Fig. 1. Specific layer wave impedance can be determined as follows:[9,12]

$$Z_f = \frac{k_s n_j \cos\theta}{\omega\varepsilon_j^2}. \tag{4}$$

In Eq. (4), n_j and ε_j are RI and permittivity of j'th (specific) layer, $\omega = 2\pi c/\lambda$ and k_s is the light wave vector defined by Eq. (8). The variables A, B, C, and D in Eq. (3) that can be calculated by solving the following matrix equation as follows:[9,12]

$$\begin{bmatrix} A & B \\ C & D \end{bmatrix} = \begin{bmatrix} A_2 & B_2 \\ C_2 & D_2 \end{bmatrix}\begin{bmatrix} A_3 & B_3 \\ C_3 & D_3 \end{bmatrix}\begin{bmatrix} A_4 & B_4 \\ C_4 & D_4 \end{bmatrix}\cdots\begin{bmatrix} A_{N-1} & B_{N-1} \\ C_{N-1} & D_{N-1} \end{bmatrix}. \tag{5}$$

Equation (5) shows n'th layer system constants. Here, the first layer represents reflectance, and consequently, it is misplaced in the matrix equation. In matrix, each element describes the reflection of the specific layer. These are the subscripted variables A, B, C, and D of each matrix and can be found:[9,12]

$$\left.\begin{aligned} A_j &= \cos(d_j\omega\varepsilon_j^2\cos\theta_j) \\ B_j &= Z_j\cos(d_j\omega\varepsilon_j^2\cos\theta_j) \\ C_j &= \frac{\sin(d_j\omega\varepsilon_j^2\cos\theta_j)}{Z_j} \\ D_j &= \cos(d_j\omega\varepsilon_j^2\cos\theta_j) \end{aligned}\right], \tag{6}$$

where d_j, θ_j, and Z_j are thickness, angle of incidence, and wave impedance of the j'th layer, respectively. The angle of incidence of j'th layer is unknown that can be found as a function of the RI of the initial and j'th layer as follows:[12]

$$\theta_j = \cos^{-1}\left[\sqrt{1 - \frac{n_i}{n_j}\sin\theta^2\theta_j}\right]. \tag{7}$$

The light generated an evanescent wave normally known as SPW, when travels through prism and is reflected at the prism–gold–graphene interface.[12] The SPW propagation constant (k_{SPW}) that propagates along the horizontal direction is described in Eq. (8), where n_{Au} is the RI of the gold and n_s is the RI of the sample:[12]

$$k_{\mathrm{SPW}} = \frac{2\pi}{\lambda_{633}}\sqrt{\frac{n_{\mathrm{Au}}^2 n_S^2}{n_{\mathrm{Au}}^2 + n_S^2}}. \tag{8}$$

The SPR applications concerned of real RI changes owing to biomolecule interaction and enterprise to the change in SPW.[11–14] SPW propagates indifferent propagation constant of incident light, which is known as surface plasmon resonance point (SPRP).[9,12,33] The frequency at SPRP is called SRF. If SPW changes, it makes the SRF change, which is given in the following:[12]

$$\mathrm{SRF} = \frac{k_{\mathrm{SPW}} C}{2\pi\sqrt[3]{n_{\mathrm{Au}} n_S n_G}}, \tag{9}$$

where c is light speed. Transmittance versus SRF curve is normally known as surface plasmon resonance frequency (SPRF) response curvature. Here, four layered Fresnel model is applied to create an SPRF curve for the proposed fiber optic SPR sensor to determine transmitted light intensity. The reflectance versus angle of incidence or reflectance versus wavelength characteristics curve is known as the SPR curve. The SPR angle that can be represented as follows:[12]

$$\theta_{\mathrm{SPR}} = a \sin\left(\frac{1}{n_P}\sqrt{\frac{n_{\mathrm{Au}}^2 n_s^2}{(n_{\mathrm{Au}}^2 + n_s^2)}}\right). \tag{10}$$

The shifting characteristics of the SPR angle and SRF owing to the change of RI are established as the following equation:[9–11]

$$n_s^2 = n_s^1 + c_a \frac{dn}{dc}. \tag{11}$$

Equation (11) shows how RI of the sensing medium is changed after the hybridization between sh-DNA and mr-DNA sequences. The SPR angle and SRF are RI-dependent parameter of sensing medium. Here, n_s^1 is the RI of the sensing dielectric before adsorption of sh-DNA molecule. When dielectric sample (probe or target) is absent inside the sensing medium, then n_s^1 is the RI of PBS saline ($n_4 = 1.34$), which is available in bare sensor. C_a is the concentration of adsorbed bio molecules, for example, if 1000 nM concentrated mr-DNA has been added into the sensing medium, then the value of $C_{\mathrm{a}} = 1000$ nM. The $\frac{dn}{dc}$ is the RI increment parameter, suppose, after adding 1000 nM concentrated molecules, the RI of the sensing layer has been changed because the sensing layer now consists not only PBS but also 1000 nM concentrated molecules. The changed value of RI from PBS is $\frac{dn}{dc}$ (=0.181 $\mathrm{cm}^3/\mathrm{gm}$ for PBS as bare case[12]). And n_s^2 is the RI of the sensing dielectric after adsorption of mr-DNA. PBS is made by containing 0.0003 mol of NaH_2PO_4 (monosodium phosphate), 0.0016 mol of Na_2HPO_4 (disodium phosphate), 0.022 mol of NaCl, and 0.00054 mol of KCl mixing in Milli-Q water.[29] PBS buffer solution allows easy discrimination of perfectly matched DNA from mismatch DNA sequences.[29] The RI increment parameter is a (dn/dc) value of 0.18 ± 0.03 cm^3/g, irrespective of the identity of the protein and the buffer ions in the occasion of utilizing PBS buffer solution.[28] The sensitivity of the optical SPR sensor is defined as the ratio of the change of output parameters (SRF or θ_{SPR}) to the change in the concentration of biomolecules, ΔC_{a}.[9,12]

2.2 *Designated DNA Sequences for Detection of Breast Cancer*

In this study, we selected 916delTT and 6174delT specific mutations in BRCA-1 and BRCA-2 genes, respectively, for the detection of breast cancer. Mutated type (mr) oligonucleotide, wild-type (wt) oligonucleotide, immobilization mutant (sh), and control target (mf) oligonucleotide represent complementary DNA sequence, mismatch DNA sequence, immobilization p-DNA sequence, and control target DNA sequence, respectively. These sequence orientation specification data in 916delTT and 6174delT are tabulated in Tables 1 and 2, respectively.[2,31,34]

In Tables 1 and 2, p-DNA sequence (sh-DNA), target fully complementary sequence (mr-DNA), and target mismatch sequence (wt-DNA) are shown in bold, italic, and bold italic, respectively, whereas control target sequence (mf-DNA) is revealed in black.

Perfectly matched hybridization event between sh-DNA sequence and mr-DNA sequence in 916delTT and 6174delT specific mutations in BRCA-1 and BRCA-2 genes revealed the biomarker of genetic breast cancer, shown in Figs. 2(a) and 3(a), respectively.

Table 1 Sequence orientation of adenine (A), thymine (T), guanine (G), and cytosine (C) sequence in of BRCA1 (916delTT).

Immobilized mutant (sh) sequence	5′-SH-$(CH_2)_6$-TTT TTT TTT TTT TTT **GTT CTG TCA AACT**-3′
Mutated type (mr) target sequence	5′-TGC CAC ATG GCT CCA CAT GCA *AGT TTG ACA GAA C*TA CCC TGA TAC TTT TCT GGA TGCC-3′
Wild type (wt) target sequence	5′-TGC CAC ATG GCT CCA CAT GCA *AGT TTG A**AA CA**G AAC* TAC CCT GAT ACT TTT CTG GAT GCC-3′
Control target (mf) sequence	5′-GGC ATC CAG AAA AGT ATC AGG GTA GTT CTG TTT CAA ACT TGC ATG TGG AGC CAT GTG GCA-3′

Table 2 Sequence orientation of adenine (A), thymine (T), guanine (G), and cytosine (C) sequence in BRCA2 (6174delT).

Immobilized mutant (sh) sequence	5′-AGC TGG TCT **GAC GTT TAT GAA** TGT TCG TTACT-3′
Mutated type (mr) target sequence	5′-GGTA CGA CAC GAT TTT TAG GGAC *TTC ATA AAC GTC* TAC TCT GAC-3′
Wild type (wt) target sequence	5′-GGTA CGA CAC GAT TTT TAG GGAC *TTC AT**C** **G**AC **A**TC* TAC TCT GAC-3′
Control target (mf) sequence	5′-GTC AGA GTA GAT GTC GAT GAA GTC CCT AAA AAT CGT GTC GTACC-3′

On the other hand, Figs. 2(b) and 3(b) are the figural representation of mismatched hybridization event between wt-DNA sequence and mr-DNA sequence in 916delTT and 6174delT specific mutations in BRCA-1 and BRCA-2 genes, which revealed the biomarker of no possibility of genetic breast cancer. This mismatched and perfectly matched hybridization between sh-DNA sequence to mr-DNA sequence and sh-DNA sequence to wt-DNA sequence are numerically performed at concentrations ranging from 1 to100 nM in PBS solution. Mf-DNA, HCL, and the appropriate chemical have flowed with PBS solution with eliminating mr-DNA and wt-DNA samples and generating sh-DNA sample.[23]

3 Numerical Results and Discussion

3.1 *Sensor Detection Consideration*

The addition of sh-DNA sequence as p-DNA on the sensing layer, reflectance versus SPR angle ($R_{\mathrm{min}} \sim \theta_{\mathrm{SPR}}$), and transmittance versus SRF ($T_{\mathrm{max}} \sim$ SRF) curve shift rightward. This is due to the addition of a probe changes the RI of the sensing dielectric medium (PBS in bare). By insertion of electron-rich DNA molecules, the number of carriers of graphene layer changes, which leads to modification of the propagation constant of SPW described in Eq. (8). Finally, a change in SRF is found due to the modification of the propagation constant of SPW described in Eq. (9). Therefore, the proposed SPR sensor with high performance is successfully

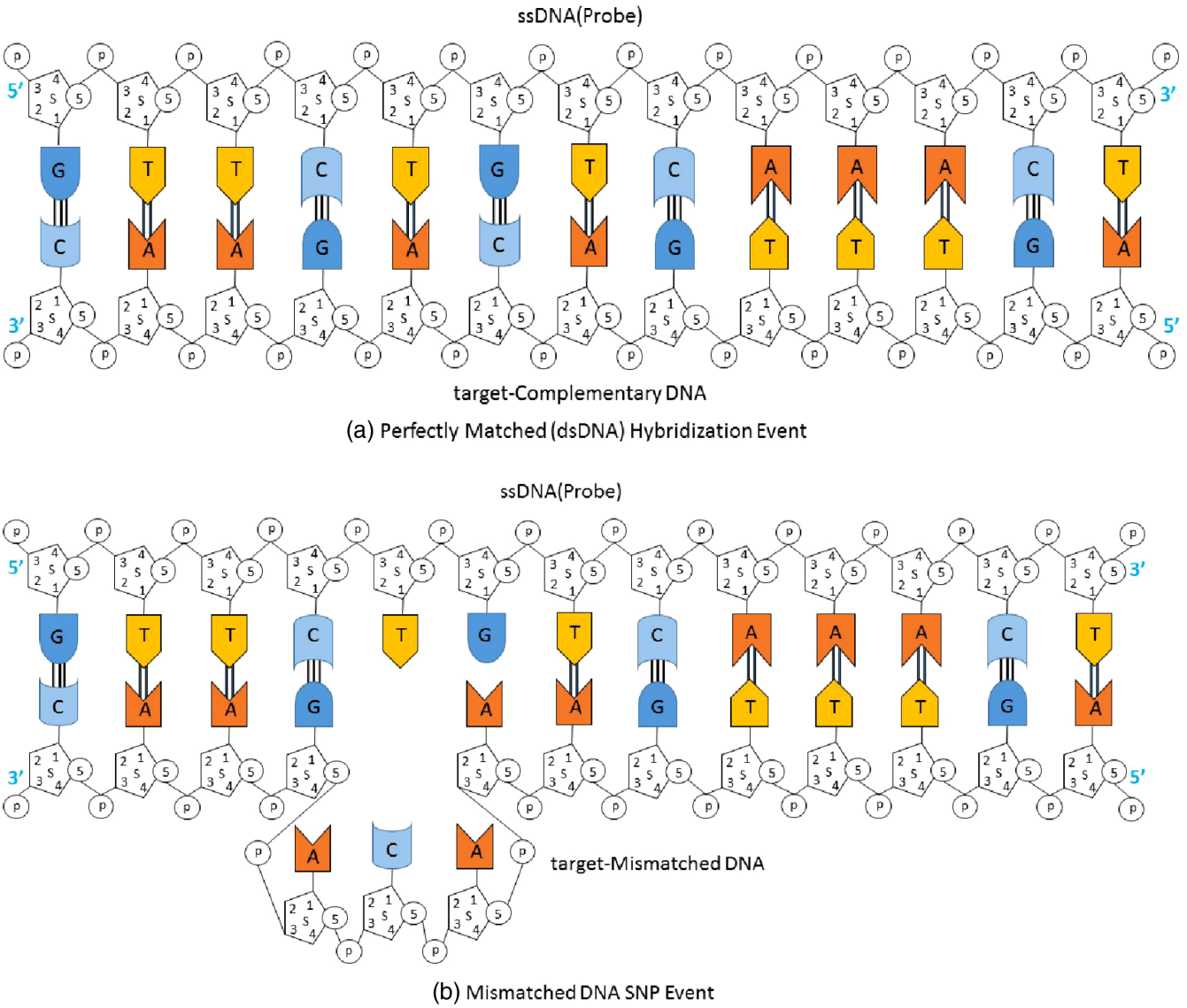

Fig. 2 (a) Figural orientation between sh-DNA and mr-DNA sequence of BRCA-1 gene (916delTT): perfectly matched hybridization happened (A–T bond by dihydrogen bonding, G–C bond by trihydrogen bonding). (b) Figural orientation between sh-DNA and wt-DNA sequence: mismatch hybridization happened.

used to detect early breast cancer by observing the hybridization nature (perfectly matched or mismatched) based on the SPR angle and SRF variations. It is observed from Figs. 4(a) and 4(b) by adding sh-DNA as p-DNA (denoted by dip-blue color line), on the graphene surface, the SPR angle and SRF are considerably right shifted by 1.10^0 THz (from 57.75^0 to 58.80^0) and 1.04 THz (from 92.34 THz to 93.38 THz), respectively. This phenomenon can illustrate the dependency of SPR angle, an SRF on the immobilization of the p-DNA, and hybridization of the complementary target DNA (mr-DNA in this work).

In Figs. 4(a) and 4(b), light green color line shows the change of SPR angle and SRF, respectively, with the submersion of the wt-DNA as mismatch target-DNA to the immobilized probe (sh-DNA) on SPR device. The results reveal that the SPR angle and SRF are 58.84^0 and 93.94 THz, respectively, after submersion of mismatched DNA (wt-DNA in this work). These values indicate no significant change in the SPR angle (the change of the SPR angle while emerging mismatched target is $\Delta\text{SPR} = 0.04^0$) as well as no significant change in the SRF (the change of SRF while emerging mismatched target is $\Delta\text{SRF} = 0.56$ THz). When the sh-DNA sequence is contacted with wt-DNA sequence, there is no hydrogen bonding between the sh-DNA and wt-DNA strands according to Figs. 2(b) and 3(b) in 916delTT and 6174delT specific mutations in BRCA-1 and BRCA-2 genes, respectively, because of the presence of a mismatched pair. Therefore, there is no change of charges in the sensing medium due to its nonbonding reaction between two pairs of DNA strands since they cannot be hybrid. This information reveals that there is no possibility of genetic breast cancer.

Figures 4(a) and 4(b) also show the $R_{\min} \sim$ SPR angle and $T_{\max} \sim$ SRF characteristics, respectively, of the proposed model for different concentrated target DNA (mr-DNA), where each color line represents individual concentration of mr-DNA molecules. Here, black line shows $R_{\min} \sim$ SPR

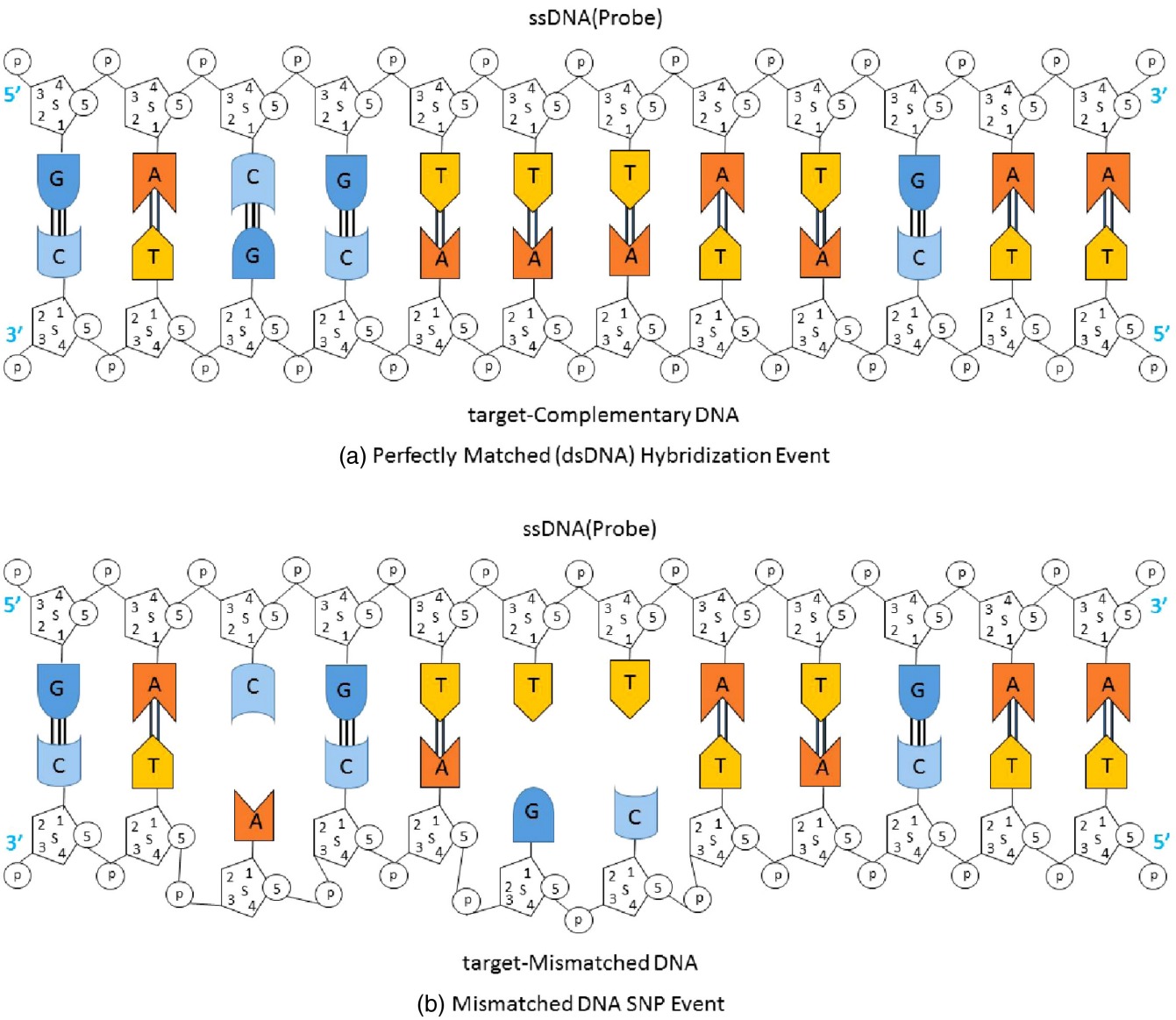

Fig. 3 (a) Figural orientation between sh-DNA and mr-DNA sequence of BRCA-2 gene (6174delT): perfectly matched hybridization happened (A–T bond by dihydrogen bonding, G–C bond by trihydrogen bonding). (b) Figural orientation between sh-DNA and wt-DNA sequence: mismatch hybridization happened.

angle and $T_{max} \sim$ SRF characteristics curve after addition of 1500 nM perfectly matched mr-DNA, red line shows $R_{min} \sim$ SPR angle and $T_{max} \sim$ SRF characteristics curve after addition of 1525 nM perfectly matched mr-DNA, light blue line shows $R_{min} \sim$ SPR angle and $T_{max} \sim$ SRF characteristics curve after addition of 1550 nM perfectly matched mr-DNA, yellow line shows $R_{min} \sim$ SPR angle and $T_{max} \sim$ SRF characteristics curve after addition of 1575 nM perfectly matched mr-DNA, and magenta color line shows $R_{min} \sim$ SPR angle and $T_{max} \sim$ SRF characteristics curve after addition of 1600 nM perfectly matched mr-DNA, respectively. The results reveal that the SPR angles are 59.10^0, 59.15^0, 59.20^0, 59.30^0, and 59.35^0 as well as the SRF are 94.90 THz, 94.99 THz, 95.10 THz, 95.22 THz and 95.36 THz respectively, for the five cases. According to these analytical data, four important factors—the SPR angle, the minimum reflectance, the SRF, and the maximum transmittance—play a significant role in detecting early breast cancer by observing DNA hybridization events. The sensing parameter R_{min}, θ_{SPR}, SRF, and T_{max} changes with different concentrated mr-DNA and wt-DNAs (ranging 1 to 100 nM) is figured in the Figs. 4(a) and 4(b), furthermore, table data have been extracted in Table 3. It is evidently decided that the significant right shift of θ_{SPR} and SRF curve is a sign of perfectly matched hybridization happened in 916delTT and 6174delT,[34] which reveals mutations in 916delTT and 6174delT biomarkers in BRCA1 and BRCA2, respectively.

Figures 4(a) and 4(b) realistically explain the $R_{min} \sim \theta_{SPR}$ (SPR curve) characteristics and $T_{max} \sim$ SRF (SPRF curve) characteristics, respectively, without p-DNA, with p-DNA, and flowing the specific concentrated complementary target wt-DNA or mr-DNAs of BRCA-1 and BRCA-2 genes. The RI is changed owing to the immobilization of different concentrated breast cancer biomarker (916delTT and 6174delT)

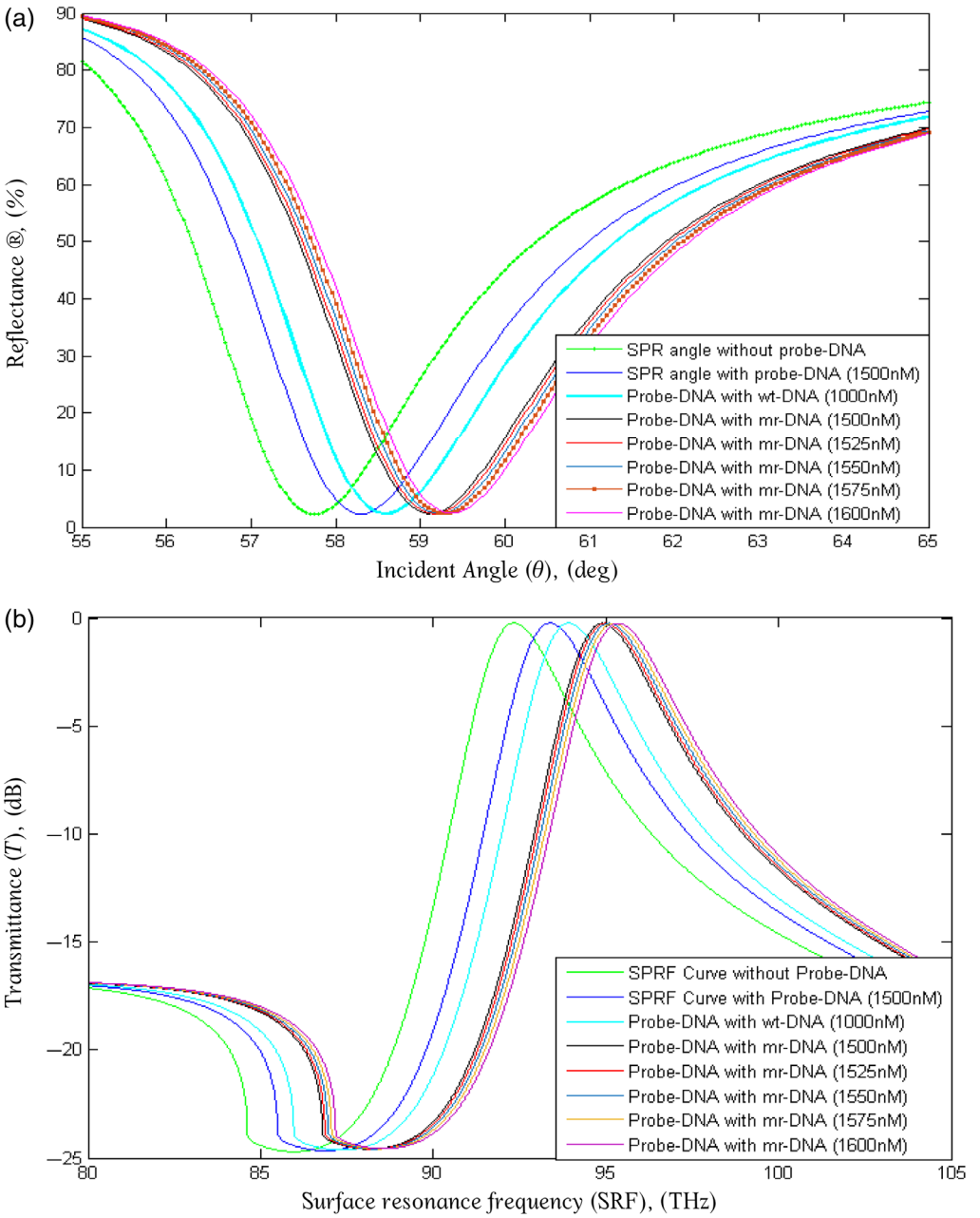

Fig. 4 (a) The SPR curves characteristics. (b) The SPRF curves characteristics of SPR sensor without p-DNA, with p-DNA, and flowing the different concentrated complementary target wt-DNA or mr-DNA of BRCA-1 and BRCA-2 genes in PBS.

DNA molecules. The RI of detecting medium has a significant impact on the SPRF and the SPR curve. The significant right shift of θ_{SPR} and SRF is a sign of recognition of specific mutations 916delTT and 6174delT interaction with p-DNAs, as well as that clarifies the detection of hereditary breast cancer. The detecting parameter changes with differently concentrated mr-DNAs have been tabulated in Table 3, accordingly, a decision will be made based on the change of detecting parameter.

In Table 3, the breast cancer recognizing attributors (δR_{min}, $\delta\theta_{\mathrm{SPR}}$, δT_{max}, and δSRF) are calculated by choosing the change of R_{min}, θ_{SPR}, T_{max}, and SRF value after adding p-DNA as standard. And after adding p-DNA, the interaction between p-DNA to mismatched (wt sequence) DNA and p-DNA to different concentrated perfectly matched target (mr sequence) DNAs has been determined and tabulated in Table 4, in order to make a decision according to Table 5. The following Eq. (12) is used to determine standard attributor's value, in which value is essential for proper detection of genetic biomarkers (916delTT and 6174delT) for early breast cancer recognized specific mutations of BRCA-1 and BRCA-2 genes as follows:

$$\left.\begin{aligned}
\delta R_{\mathrm{min}}^{\mathrm{Cancer}} &= |R_{\mathrm{min}}^{\mathrm{probe}} - R_{\mathrm{min}}^{mr=1500}| = 0.09 \\
\delta\theta_{\mathrm{SPR}}^{\mathrm{Cancer}} &= |\theta_{\mathrm{SPR}}^{\mathrm{probe}} - \theta_{SPR}^{mr=1500}| = 0.80 \text{ deg}. \\
\delta T_{\mathrm{max}}^{\mathrm{Cancer}} &= |T_{\mathrm{max}}^{\mathrm{probe}} - T_{\mathrm{max}}^{mr=1500}| = 0.0083 \text{ dB} \\
\delta \mathrm{SRF}^{\mathrm{Cancer}} &= |\mathrm{SRF}^{\mathrm{probe}} - \mathrm{SRF}^{\mathrm{mr=1500}}| = 1.52 \text{ THz}
\end{aligned}\right\}. \quad (12)$$

Table 3 Data of change of detecting attributors (δR_{min}, $\delta\theta_{SPR}$, δT_{max}, and δSRF) for introducing different concentrated target WT-DNA or MR-DNA of BRCA-1 and BRCA-2 gene.

Concentration (C_a) (nM)	R_{min} (%)	θ_{SPR} (deg)	T_{max} (dB)	SRF (THz)	$\delta R_{min}^{P-T} = \lvert R_{min}^{probe} - R_{min}^{target} \rvert$	$\delta\theta_{SPR}^{P-T}(deg) = \lvert\theta_{SPR}^{probe} - \theta_{SPR}^{target}\rvert$	$\delta T_{max}^{P-T}(dB) = \lvert T_{max}^{probe} - T_{max}^{target}\rvert$	$\delta SRF^{P-T}(THz) = \lvert SRF^{probe} - SRF^{target}\rvert$
0 (no-sh-DNA)	2.26	57.75	0.2288	92.34	—	—	—	—
1500 (sh-DNA)	2.31	58.80	0.2339	93.38	0.00	0.00	0.0000	0.00
1000 (wt-DNA)	2.34	58.84	0.2368	93.94	0.03	0.04	0.0029	0.56
1500 (mr-DNA)	2.40	59.10	0.2422	94.90	0.09	0.80	0.0083	1.52
1525(mr-DNA)	2.40	59.15	0.2427	94.99	0.09	0.85	0.0088	1.61
1550 (mr-DNA)	2.41	59.20	0.2433	95.10	0.10	0.90	0.0094	1.72
1575 (mr-DNA)	2.42	59.30	0.2441	95.22	0.11	1.00	0.0102	1.84
1600 (mr-DNA)	2.42	59.35	0.2449	95.36	0.11	1.05	0.0110	1.98

Table 4 Decision making based upon different situations that happened to detecting attributors.

Pathology no.	Decision making condition (with respect to change of R_{min}, θ_{SPR}, T_{max}, and SRF)			Decision
01	$\delta R_{min}^{P-T} \geq \delta R_{min}^{Cancer}$ && $\delta\theta_{SPR}^{P-T} \geq \delta\theta_{SPR}^{Cancer}$	OR	$\delta T_{max}^{P-T} \geq \delta T_{max}^{Cancer}$ && $\delta SRF^{P-T} \geq \delta SRF^{Cancer}$	Cancer detect
02	$\delta R_{min}^{P-T} < \delta R_{min}^{Cancer}$ && $\delta\theta_{SPR}^{P-T} < \delta\theta_{SPR}^{Cancer}$		$\delta T_{max}^{P-T} < \delta T_{max}^{Cancer}$ && $\delta SRF^{P-T} < \delta SRF^{Cancer}$	No cancer detect
03	$\delta R_{min}^{P-T} \geq \delta R_{min}^{Cancer}$ && $\delta\theta_{SPR}^{P-T} \leq \delta\theta_{SPR}^{Cancer}$		$\delta T_{max}^{P-T} \leq \delta T_{max}^{Cancer}$ && $\delta SRF^{P-T} \geq \delta SRF^{Cancer}$	Further try again
04	$\delta R_{min}^{P-T} \leq \delta R_{min}^{Cancer}$ && $\delta\theta_{SPR}^{P-T} \geq \delta\theta_{SPR}^{Cancer}$		$\delta T_{max}^{P-T} \geq \delta T_{max}^{Cancer}$ && $\delta SRF^{P-T} \leq \delta SRF^{Cancer}$	Further try again

Table 5 Data of R_{min}, θ_{SPR}, T_{max}, and SRF without graphene layer and with the total number of increasing graphene layer in fiber optic SPR biosensor.

Graphene layer	R_{min} (%)	θ_{SPR} (deg)	T_{max} (dB)	SRF (THz)	δR_{min} [%]	$\delta\theta_{SPR}$ [deg]	δT_{max} [dB]	δSRF [THz]
Without layer (£ = 0 nm)	0.25	57.35	0.0252	91.92	0.00	0.00	0.0000	0.00
First layer (£ = 1 × 0.34 nm)	2.26	57.70	0.2285	92.28	2.01	0.35	0.2033	0.36
Second layer (£ = 2 × 0.34 nm)	5.40	58.10	0.5550	92.68	5.15	0.75	0.5298	0.76
Third layer (£ = 3 × 0.34 nm)	9.05	58.50	0.9481	93.08	8.80	1.15	0.9229	1.16
Fourth layer (£ = 4 × 0.34 nm)	12.87	58.95	1.3770	93.51	12.62	1.60	1.3518	1.59
Ninth layer (£ = 9 × 0.34 nm)	30.51	61.50	3.6405	95.93	30.26	4.15	3.6153	4.01
Tenth layer (£ = 10 × 0.34 nm)	33.55	62.10	4.0867	96.47	33.30	4.75	4.0615	4.55

Equation (12) describes that breast cancer recognizing attributors minimum value is stated in such way that is equal to the right shift of SPR and SRF curvatures after submersing mutated type target (1500 nm concentrated mr sequence) DNA into p-DNA. Concededly, Table 4 is the decision-making table, which can be applied for breast cancer detection, taking advantage of the detecting attributor's values. The minimum attributor values are $\delta R_{min}^{Cancer} = 0.09\%$, $\delta\theta_{SPR}^{Cancer} = 0.80$ deg, $\delta T_{max}^{Cancer} = 0.0083$ dB, and $\delta SRF^{Cancer} = 1.52$ THz for detection of specific mutations in PBS solutions.

Table 4 represents the pathological decision for different cases. After submersing an arbitrary molecular sample on the sensing region of SPR device, either perfectly matched sequence (mutated type target sequence, mr-DNA) or mismatched sequence (wild-type target sequence, wt-DNA) in 916delTT and 6174delT with two specific mutations in BRCA-1 and BRCA-2 genes, the detecting attributors—such as R_{min} (%), θ_{SPR} (deg), T_{max} (dB), and SRF (THz)—are changed according to the nature of hybridization. When the change of δR_{min}^{P-T}, $\delta\theta_{SPR}^{P-T}$, δT_{max}^{P-T}, and δSRF^{P-T} are greater than or equal to δR_{min}^{Cancer}, $\delta\theta_{SPR}^{Cancer}$, δT_{max}^{Cancer}, and δSRF^{Cancer},

then specific mutations (916delTT and 6174delT) of BRCA-1 and BRCA-2 genes are sensed (breast cancer detect) by SPR sensor (described this decision by pathology No. 01 in Table 4) and if the change of $\delta R_{\min}^{P-T}$, $\delta\theta_{\mathrm{SPR}}^{P-T}$, $\delta T_{\max}^{P-T}$, and $\delta\mathrm{SRF}^{P-T}$ is smaller than $\delta R_{\min}^{\mathrm{Cancer}}$, $\delta\theta_{\mathrm{SPR}}^{\mathrm{Cancer}}$, $\delta T_{\max}^{\mathrm{Cancer}}$, and $\delta\mathrm{SRF}^{\mathrm{Cancer}}$, then it confirms that no breast cancer mutations are sensed (described this decision by pathology No. 02 in Table 4); apart from both of these decisions, no consistencies consequence will be recognized. Hence, the change of $\delta R_{\min}^{P-T}$, $\delta\theta_{\mathrm{SPR}}^{P-T}$, $\delta T_{\max}^{P-T}$, and $\delta\mathrm{SRF}^{P-T}$ is due to the variability arising from other interferents in the biomolecules and the recognition process should be further tried again (described this decision by pathology Nos. 03 and 04 in Table 4). In such way, a graphene-implicated SPR sensor is used to make a pathological decision from the achieved results, respectively, Table 4 and its pathology nos. indicated the detection and can be utilized for confirming detection of 916delTT and 6174delT mutation.

3.2 *Sensor Performance Consideration*

In this section, a numerical study is presented on the effect of including the graphene layer in terms of SPR curve ($R_{\min}$ versus θ_{SPR}) and SRF curve ($T_{\max}$ versus SRF) characteristics. Here, we used PBS solution ($n_4 = 1.34$) before adsorbing probe sh-DNA molecules. The θ_{SPR} and SRF without the graphene layer are 57.35 deg and 91.92 THz, furthermore, with a single layer of graphene is 57.70 deg and 92.28 THz, respectively, shown in Figs. 5(a) and 5(b). The SPR angle (change of SPR angle, $\delta\theta_{\mathrm{SPR}} = 0.35$ deg) and SRF (change

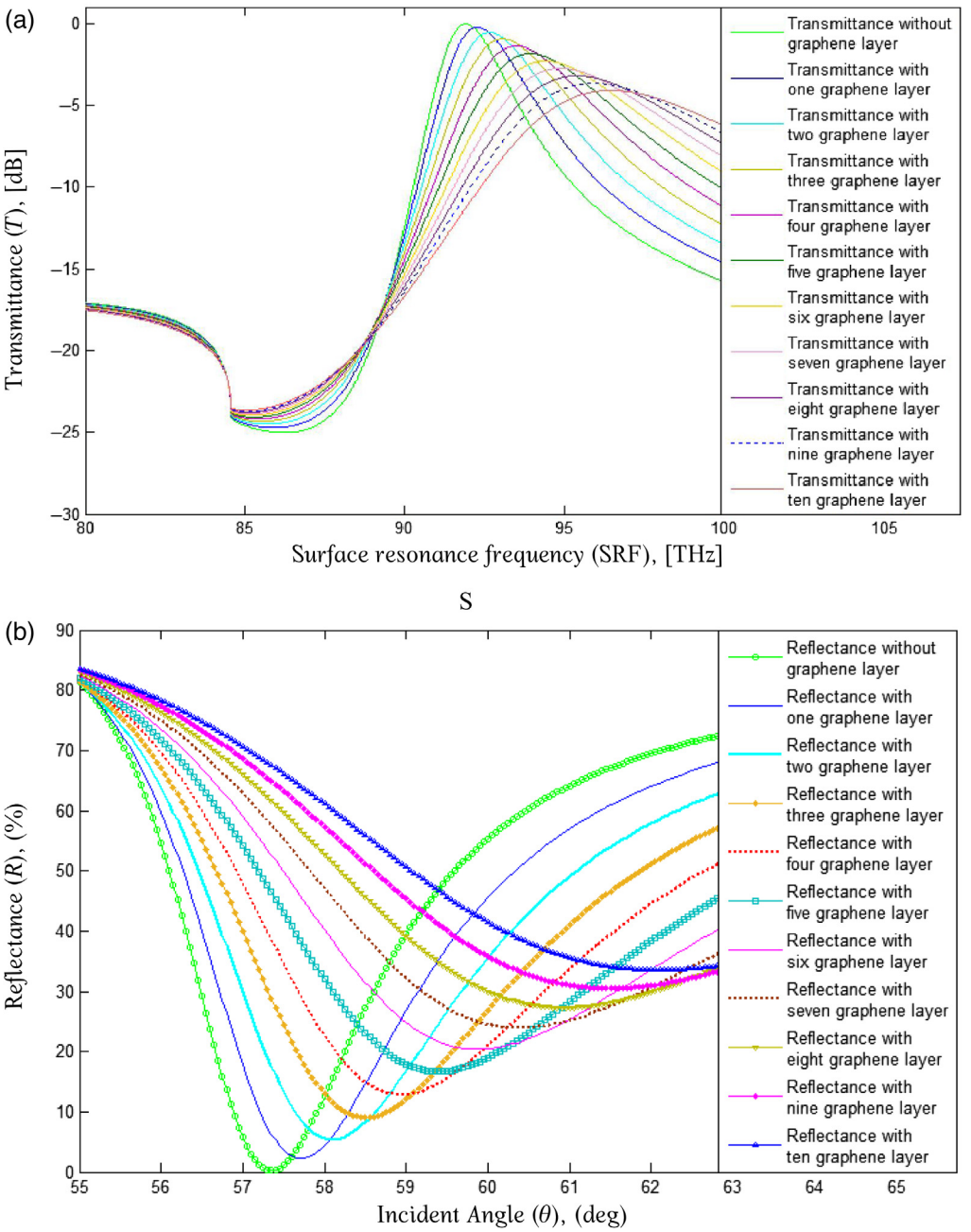

Fig. 5 (a) The SPR curves. (b) The SPRF curves for the fiber optic SPR biosensor without graphene and with graphene implicated sensor (for £ = 1,2, 3, . . . , 10) before the adsorption of target BRCA DNA molecules.

of SRF, $\delta\text{SRF} = 0.36$ THz) have been increased owing to adding graphene film, which is enhanced the sensitivity of this sensor. This enhanced sensitivity is due to the electron loss of graphene, high carrier mobility, high optical transparency, exceptional mechanical flexibility, strength,[35] low resistivity, tunable conductivity, and extreme mode confinement,[25–27] which is accompanying the imaginary dielectric constant. This increased SPR angle will lead to increased sensitivity of the sensor as sensitivity is directly related to the variation of SPR angle discussed in Refs. 8–15. And thus, the detecting attributors $\delta\theta_{\text{SPR}}$ and δSRF are shifting rightward because of adding the graphene layer. These values have been tabulated in Table 5, as well as table data depicted in Figs. 5(a) and 5(b), respectively.

In Table 3, the breast cancer recognizing attributors $R_{\min}$, θ_{SPR}, $T_{\max}$, and SRF are increasing with the number of the graphene layer ($£ = n * 0.34$ nm; $1 \leq n \leq 10$) included on the Au thin film, which causes enhanced sensitivity of the proposed fiber optic SPR sensor.

The sensor performance is determined in terms of sensor sensitivity (S). Sensor sensitivity is defined as function to the change of output (change of $\Delta\theta_{\text{SPR}}$ or ΔSRF) with respect to the change of input (concentration of the sensing layer, ΔC_{a}).[9]

For $R_{\min} \sim$ SPR angle attributor, sensitivity (S) is defined as follows:[12]

$$\left.\begin{aligned} S &= \frac{\Delta\theta_{\text{SPR}}}{\Delta c_a} \\ &= \frac{\Delta\theta^0_{\text{SPR}} + \Delta\theta^L_{\text{SPR}}}{\Delta c_a} \\ &= \frac{\Delta\theta^0_{\text{SPR}} + 0.35\Delta\theta^0_{\text{SPR}}}{\Delta c_a} \\ &= \frac{(1+0.35L)\Delta\theta^0_{\text{SPR}}}{\Delta c_a} \\ &= (1 + 0.35L)s^O \end{aligned}\right], \tag{13}$$

where $\Delta\theta_{\text{SPR}}$ is the change of SPR angle due to the presence of mr-DNA sequence and Δc_a is the change of concentration of the sensing dielectric after adsorption of perfectly matched mr-DNA molecule. Here, S^0 is the sensitivity without graphene, and S^L is the sensitivity with graphene. Equation (13) is derived from Table 5 and is seen if we use a single graphene layer ($£ = 1, 0.34$ nm), the sensitivity has been increased 35% more with respect to conventional sensor.

For $T_{\max} \sim$ SRF attributor, sensitivity (S) is defined as follows:[9]

$$\left.\begin{aligned} S &= \frac{\Delta\text{SRF}}{\Delta c_a} \\ &= \frac{\Delta\text{SRF}^0 + \Delta\text{SRF}^L}{\Delta c_a} \\ &= \frac{\Delta\text{SRF}^0 + 0.36\Delta\text{SRF}^0}{\Delta c_a} \\ &= \frac{(1+0.35L)\Delta\text{SRF}^0}{\Delta c_a} \\ &= (1 + 0.36L)s^O \end{aligned}\right], \tag{14}$$

where ΔSRF is the SRF change of sensor summing with and without graphene sublayers, $S0$ is the sensitivity of the devices without graphene film, and SG is the sensitivity for different number of graphene sublayers ($L = 1,2,3,\ldots$). Equation (14) is derived from Table 5 and is seen if we use a single graphene layer ($£ = 1, 0.34$ nm), the sensitivity has been increased 36% more with respect to conventional sensor.

4 Conclusion

We present a numerical modeling of graphene-coated fiber optic SPR biosensor for proper detection of genetic biomarkers (916delTT and 6174delT) for early breast cancer by means of DNA hybridization. From the variation of the SPR angle and SRF, the proposed sensor can differentiate between perfectly matched and mismatched DNA interaction between p-DNA (sh-DNA mutant) and target DNA (mutation type mr-DNA). Numerical results show that the use of graphene can be more sensitive compared with the usual SPR biosensors. This increased sensitivity is due to the absorption ability of graphene. This sensor provided the easiest way of monitoring cancer tumor cell and confirming detection of specific mutations of BRCA-1 and BRCA-2 genes. The thought offered in this article is expected to be understood easily, and because of enhanced sensitivity, the proposed hybrid SPR biosensor has great prospective in future industrial applications of genetic biomarkers (916delTT and 6174delT) for early breast cancer detection.

Acknowledgments

The authors declare that they have no conflicts of interest.

References

1. D. A. Caporale and E. E. Swenson, "Two different BRCA2 mutations found in a multigenerational family with a history of breast, prostate, and lung cancers," *Adv. Genomics Genet.* **4**, 87–94 (2014).
2. L. G. Carrascosa, A. Calle, and L. M. Lechuga, "Label-free detection of DNA mutations by SPR: application to the early detection of inherited breast cancer," *Anal. Bioanal. Chem.* **393**(4), 1173–1182 (2009).
3. S. D. Dufresne et al., "BRCA1 and BRCA2 mutation screening using smart cycler II high-resolution melt curve analysis," *Arch. Pathol. Lab. Med.* **130**(2), 185–187 (2006).
4. C.-W. Lin and C.-C. Chang, "Breast cancer detection using surface plasmon resonance-based biosensors," in *Biosensors and Cancer*, P. T. Cagle, Ed., p. 17, College of American Pathologists (2011).
5. I. Godet and D. M. Gilkes, "BRCA1 and BRCA2 mutations and treatment strategies for breast cancer," *Integr. Cancer Sci. Ther.* **4**(1), 1–7 (2017).
6. Y. Li et al., "Single-nucleotide polymorphism genotyping by nanoparticle-enhanced surface plasmon resonance imaging measurements of surface ligation reactions," *Anal. Chem.* **78**(9), 3158–3164 (2006).
7. M. R. Hasan et al., "Design of a surface plasmon resonance refractive index sensor with high sensitivity," *Opt. Eng.* **56**(8), 087101 (2017).
8. M. S. Anower, M. S. Rahman, and K. A. Rikta, "Performance enhancement of graphenecoated surface plasmon resonance biosensor using tungsten disulfide," *Opt. Eng.* **57**(1), 017114 (2018).
9. M. B. Hossain and M. M. Rana, "Graphene coated high sensitive surface plasmon resonance biosensor for sensing DNA hybridization," *Sens. Lett.* **14**(2), 145–152 (2016).
10. K. N. Shushama et al., "Graphene coated fiber optic surface plasmon resonance biosensor for the DNA hybridization detection: simulation analysis," *Opt. Commun.* **383**, 186–190 (2017).
11. M. S. Rahman et al., "Design and numerical analysis of highly sensitive Au-MoS_2-graphene based hybrid surface plasmon resonance biosensor," *Opt. Commun.* **396**, 36–43 (2017).
12. M. B. Hossain and M. M. Rana, "DNA hybridization detection based on resonance frequency readout in graphene on Au SPR biosensor," *J. Sens.* **2016**, 1–7 (2016).
13. M. S. Rahman et al., "Modeling of a highly sensitive MoS_2-graphene hybrid based fiber optic SPR biosensor for sensing DNA hybridization," *Optik* **140**, 989–997 (2017).
14. K. N. Shushama et al., "Sensitivity enhancement of graphene coated surface plasmon resonance biosensor," *Opt. Quantum Electron.* **49**(11), 381 (2017).
15. M. S. Rahman, M. B. Hossain, and M. M. Rana, "Sensitivity enhancement of porous silicon based SPR sensor using graphene-MoS_2 hybrid structure," in *Int. Conf. Electr., Comput. and Telecommun. Eng. (ICECTE)*, Dhaka, Bangladesh (2015).

16. A. K. Mishra, S. K. Mishra, and R. K. Verma, "Graphene and beyond graphene MoS_2: a new window in surface-plasmon-resonance-based fiber optic sensing," *J. Phys. Chem. C* **120**(5), 2893–2900 (2016).
17. M. B. Hossain, M. S. Muktadhir, and M. M. Rana, "Modeling graphene macroscopic and microscopic conductivity in the sub-cell FDTD method," in *Int. Conf. Electr. and Electron. Eng. (ICEEE)*, Rajshahi, Bangladesh (2015).
18. M. M. Rana et al., "Surface plasmon polariton propagation modeling for graphene parallel pair sheets using FDTD," in *Int. Conf. Appl. Supercond. and Electromagn. Dev. (ASEMD)*, Shanghai, China (2015).
19. B. Ruan et al., "Ultrasensitive terahertz biosensors based on Fano resonance of a graphene/waveguide hybrid structure," *Sensors* **17**(8), 1924 (2017).
20. M. Pumera, "Graphene in biosensing," *Mater. Today* **14**(7–8), 308–315 (2011).
21. M. B. Hossain and M. M. Rana, "An effective compact-FDTD wideband modeling of graphene conductivity," in *Int. Conf. Electr. Eng. and Inf. Commun. Technol. (ICEEICT)*, Dhaka, Bangladesh (2015).
22. M. B. Hossain, S. Muktadhir, and M. M. Rana, "Multi-structural optical devices modeling using graphene tri-layer sheets," *Optik* **127**(15), 5841–5851 (2016).
23. S. A. Ramezani et al., "Beam manipulating by gate-tunable graphene-based metasurfaces," *Opt. Lett.* **40**(22), 5383–5386 (2015).
24. A. K. Geim and K. S. Novoselov, "The rise of graphene," *Nat. Mater.* **6**, 183–191 (2007).
25. F. Bonaccorso et al., "Graphene photonics and optoelectronics," *Nat. Photonics* **4**, 611–622 (2010).
26. S. Farajollahi et al., "Circuit model for plasmons on graphene with one dimensional conductivity profile," *IEEE Photonics Technol. Lett.* **28**, 355–358 (2016).
27. S. A. Ramezani et al., "Analog computing using graphene-based metalines," *Opt. Lett.* **40**(22), 5239–5242 (2015).
28. V. Ball and J. J. Ramsden, "Buffer dependence of refractive index increments of protein solutions," *Biopolymers* **46**(7), 489–492 (1998).
29. L. Diéguez et al., "Effect of the refractive index of buffer solutions in evanescent optical biosensors," *Sens. Lett.* **7**(5), 851–855 (2009).
30. J. Homola and M. Piliarik, "Surface plasmon resonance (SPR) sensors," in *Surface Plasmon Resonance Based Sensors*, J. Homola, Ed., Springer, Berlin, Heidelberg, pp. 45–67 (2006).
31. J. S. del Río et al., "Lab-on-a-chip platforms based on highly sensitive nanophotonic Si biosensors for single nucleotide DNA testing," *Proc. SPIE* **6477**, 64771B (2007).
32. M. S. Rahman et al., "A novel graphene coated surface plasmon resonance biosensor with tungsten disulfide (WS_2) for sensing DNA hybridization," *Opt. Mater.* **75**, 567–573 (2018).
33. L. Wu et al., "Highly sensitive graphene biosensors based on surface plasmon resonance," *Opt. Express* **18**(14), 14395–14400 (2010).
34. A. Chakraborty et al., "Absence of 185delAG and 6174delT mutations among breast cancer patients of eastern India," *Asian Pac. J. Cancer Prev.* **16**(17), 7929–7933 (2015).
35. P. Englebienne, A. Van Hoonacker, and M. Verhas, "Surface plasmon resonance: principles, methods and applications in biomedical sciences," *J. Spectrosc.* **17**, 255–273 (2003).

Md. Biplob Hossain currently works as a lecturer in the Department of Electrical and Electronic Engineering (EEE), Jashore University of Science and Technology (www.just.edu.bd), Jashore, Bangladesh. He served as a lecturer in the Department of Electrical and Electronic Engineering (EEE), Bangladesh Army University of Engineering and Technology (www.bauet.ac.bd), Natore, Bangladesh, from August 10, 2016 to December 10, 2018. His research interests are in biomedical and bioinformatics engineering, surface plasmon resonance biosensor, plasmonic engineering, photonic senor, refractive index sensor, biomedical applications, analytical and computational electromagnetics, electromagnetic, compatibility, and graphene-based optical and nanostructural devices modeling. He has published around 20 papers in different international reputed journals and conferences proceedings, including IEEE, Elsevier, SPIE, Springer, PIER, SERSC, etc.

Tarik Bin Abdul Akib is currently with the Department of Electrical and Electronic Engineering, Bangladesh Army University of Engineering and Technology (www.bauet.ac.bd), Natore, Bangladesh. His research interests include modeling and performance of different types of biosensor.

Lway Faisal Abdulrazak received his BSc degree from the University of Omer Almokhtar and his MSc degree from the Universiti Teknologi Malaysia, both in communication engineering, in 2005 and 2007, respectively. In 2011, his PhD was awarded at the Wireless Communication Center, Faculty of Electrical Engineering, Universiti Teknolgi Malaysia/Malaysia. From 2007 to 2011, he was a research officer working on Mobile 4G Project in MCMC, CyperJaya, Malaysia, and a teaching assistance with the Wireless Communication Center, Malaysia. His research interests include communication, fiber optics, and antenna design. He is a senior member of the University Research Center, Cihan University Sulaimanyia, as well as a lecturer at the Computer Science Department at the same university and a reviewer of several journals.

Md. Masud Rana completed his PhD in electrical engineering from the University of Technology Sydney (UTS), Sydney, Australia, in 2013. He joined as a lecturer at the Department of Electrical and Electronic Engineering at RUET, Bangladesh, in 2006, and currently, he is a professor in the same university. He is a member of the Institute of Engineers, Bangladesh (IEB), and Institute of Electrical and Electronic Engineers (IEEE). He has authored and coauthored over 40 journal and conference papers. His research interests include microwave antenna design for biomedical applications, analytical and computational electromagnetics, electromagnetic compatibility, and graphene-based optical and nanostructural device modeling. Website: http://www.ruet.ac.bd/teachers/EEE.